Ionization of Atmospheric Gases Containing Ozone and Carbonyl Sulfide. Formation and Reactivity of SO^+ Ions

Fulvio Cacace,[§] Giulia de Petris,*[,§] Marzio Rosi,[†] and Anna Troiani[§]

Dipartimento di Studi di Chimica e Tecnologia delle Sostanze Biologicamente Attive dell'Università "La Sapienza", P.le Aldo Moro 5, 00185 Roma, Italy, and Dipartimento di Ingegneria Civile ed Ambientale, Sezione Tecnologie Chimiche e Materiali per l'Ingegneria, Università di Perugia, Via Duranti, 06131 Perugia, Italy

Received: October 5, 2000

Gaseous ionized carbonyl sulfide/ozone mixtures have been studied by mass spectrometric techniques and theoretical calculations. The evidence obtained points to this system as an effective route to the SO^+ ion, which in turn promotes a rich ion chemistry leading to S_nO^+ ($n = 2-5$) and S_n^+ ($n = 2-9$) ions via oligomerization processes.

Introduction

Carbonyl sulfide, COS, is the most abundant sulfur gas in the atmosphere. It is rather uniformly distributed throughout the troposphere, and it is thought to be the main source of stratospheric sulfur. In contrast with other sulfur-containing compounds that are rapidly oxidized in the troposphere, and consistent with its long lifetime of more than one year, it shows a sufficiently low reactivity to be transported into the stratosphere.[1] There, the progression from COS toward more oxidized species, such as SO, SO_2, and H_2SO_4, is driven by hydroxyl radicals, O_2 and O_3. As revealed by rocket and aircraft measurements, gaseous ions also are present in the stratosphere and the troposphere, where ionization, largely caused by lightning, radioactive emanation, and cosmic rays, produces O_2^+ by primary processes. A rich ionic chemistry is known to occur, involving in particular species that have low ionization potentials and easily undergo charge-transfer processes.[2] Gaseous ions are of additional interest in the stratosphere and troposphere as powerful probes for neutral gas detection, since selective reactions of naturally occurring ions with trace gases lead to characteristic ionic products. Surprisingly, although the importance of aerosols in climate and stratospheric ozone chemistry has recently intensified interest in sources and sinks of COS, and despite recent studies of the ionic chemistry of ozone,[3,4] the ionic chemistry of gases containing *both* COS and O_3 has not yet been investigated. We therefore have undertaken the study of ionized mixtures containing COS and O_3, diluted in atmospheric gases (O_2 and N_2), by mass spectrometric and theoretical methods. Remarkably, the evidence obtained unravelled an ion chemistry essentially promoted by the SO^+ ion, leading to the charged products, S_nO^+ ($n = 2-5$), of higher sulfur content than those obtained from the oxidation of neutral COS. Several of the S_nO^+ ions ($n = 3-5$) were experimentally detected for the first time in this study and are currently under further investigation. The result proves particularly significant, revealing that the ionic COS/O_3 system is the source of the $SO^{+\bullet}$ ion in the atmosphere, since other conceivable precursors, such as SO_2 and related sulfur-containing compounds, are rapidly converted to aerosols in the troposphere. The SO^+ ions produced in this way can subsequently react with the ubiquitous COS, yielding other sulfur-containing cations, and eventually their neutralization products.

* Corresponding author. E-mail: depetris@axrma.uniroma1.it.
[§] Università "La Sapienza".
[†] Università di Perugia.

Experimental Section

Mass Spectrometry. A ZABSpec oa-TOF mass spectrometer of EBE TOF configuration (Micromass Ltd., Manchester, UK) was used to generate the species of interest by chemical ionization (CI) performed at pressures of ca. 0.1−0.2 Torr. Typical operation conditions were as follows: accelerating voltage 8 kV, emission current 0.5 mA, repeller voltage 0 V, source temperature 150 °C. The mass-selected ions were structurally assayed by mass selected ion kinetic energy (MIKE) and collisionally activated dissociation (CAD) mass spectrometry. In the latter case, He was admitted into the collision cell at such a pressure as to reduce the beam intensity to 70% of its original value. MS/MS experiments were performed by recording the CAD/TOF spectra of mass-selected daughter ions. The kinetic energy releases were measured by the average of about 400 scans, at the energy resolution of 1.5 eV of main beam width. The Fourier transform-ion cyclotron resonance (FT-ICR) experiments were performed with a 47e Apex instrument (Bruker Spectrospin AG, Bremen, Germany) equipped with an external ion source, a pulsed valve, a cylindrical "infinity" cell,[5] and a Bayard-Alpert ionization gauge, whose readings were corrected for its different sensitivity to the gases used.[6] The ions generated in the source were transferred into the ICR cell and isolated by the standard procedure based on the "soft" ejection of all the unwanted ions. The ions were then allowed to react with the neutral reagent continuously admitted into the cell, in order to reach stationary pressures, typically of the order of 10^{-8} Torr. All chemicals were research-grade products from Aldrich Chemical Co., and were used without further purification. Ozone was prepared by passing UHP grade oxygen (Matheson 99,95 mol %) through a commercial ozonizer; it was collected in a silica trap cooled to 77 K and released by controlled warming of the trap.

Computational Details. Density functional theory, using the hybrid[7] B3LYP functional,[8] was used to localize the stationary points of the investigated systems and to evaluate the vibrational

10.1021/jp003656n CCC: $20.00
Published on Web 01/27/2001

frequencies. Although it is well known that density functional methods using nonhybrid functionals sometimes tend to overestimate bond lengths,[9] hybrid functionals such as B3LYP usually provide geometrical parameters in excellent agreement with experimental data.[10] Single point energy calculations at the optimized geometries were performed using the coupled-cluster single and double excitation method,[11] with a perturbational estimate of the triple excitations [CCSD(T)] approach,[12] in order to include extensive correlation contributions.[13] Transition states were located using the synchronous transit-guided quasi-Newton method developed by Schlegel and co-workers.[14] The 6-311+G(2d) basis set[15] was used. Zero point energy corrections, evaluated at the B3LYP/6-311+G(2d) level, were added to the CCSD(T) energies. The 0 K total energies of the species of interest were corrected to 298 K by adding translational, rotational, and vibrational contributions. The absolute entropies were calculated by using standard statistical-mechanistic procedures from scaled harmonic frequencies and moments of inertia relative to B3LYP/6-311+G(2d) optimized geometries. All calculations were performed using Gaussian 98[16] on a SGI Origin 2000 computer and a cluster of IBM RISC /6000 workstations.

Results

The Reaction of COS^+ with O_3. High-resolution chemical ionization (CI) spectra of COS were recorded with a ZABSpec oa-TOF mass spectrometer, which was equipped with a high-pressure CI source. Utilizing O_2, N_2, and O_3/O_2 or $O_3/O_2/N_2$ mixtures as the reagent gases, major peaks were observed at *m/z* 60 (COS^+) and 32 (S^+), traceable to the charge-transfer process

$$M^+ + COS \rightarrow COS^+ + M \qquad (1)$$
$$M = O_2, N_2, O_3$$

and the subsequent dissociation of the excited COS^+ ions formed. In addition, a major peak at *m/z* 48 was detected when employing O_3-containing mixtures. The peak was unambiguously identified as SO^+, conceivably formed from the reaction

$$O_3^+(O_3) + COS\ (COS^+) \rightarrow SO^+ + O_2 + CO \qquad (2)$$

whereas no $[COSO_3]^+$ complexes were observed.

Likewise, O_2^+, N_2^+, and O_3^+ ions were generated in the external CI source of the FT-ICR mass spectrometer, isolated by selective ejection techniques, and allowed to react, after a cooling period of 3 s, with COS that was admitted into the resonance cell, to a stationary pressure of 2×10^{-8} Torr. The charge-transfer reaction (1) was the only process observed from O_2^+ and N_2^+, whereas the O_3^+ ion promoted, in addition, reaction 2, as demonstrated by accurate mass measurements of the isobaric reagent and product ions.

As for the theoretical results, Figure 1 reports the computed optimized geometries of the minima localized on the potential energy surface of the $[COS-O_3]^+$ system. The total energies and frequencies are reported in Table 1, whereas the energetics of the relevant processes, computed at the CCSD(T) level, are reported in Table 2. The ion **1**, located 58.1 kcal mol^{-1} below the energy level of the reactants, can be described as an electrostatic ion−molecule complex, containing a SO^+ ion solvated by the CO and O_2 molecules. The ion **2**, less stable than **1** by 28.2 kcal mol^{-1}, results from a two-center coordination of two oxygen atoms of ozone with the carbon and sulfur atoms of COS, and can isomerize to the ion **3**, which is more stable

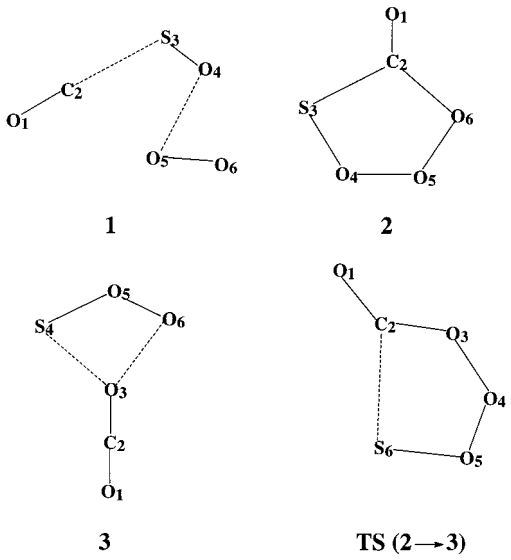

Figure 1. Optimized geometries of the localized minima on the potential energy surface of the COS^+/O_3 system. TS(**2** → **3**) is the transition state for the **2** → **3** isomerization.

by 6.0 kcal mol^{-1} than **1**. The transition state for the **2** → **3** isomerization is also illustrated in Figure 1.

The Reaction of SO^+ with COS. In the high-pressure O_3 chemical ionization of COS, $[COS-SO]^+$ and $[COS-S_2O]^+$ adducts were observed and structurally assayed by MIKE, CAD, and MS^3 spectrometry. In particular, the elemental composition of the ions assayed, as well as of their decomposition products, was assigned on the basis of the combined information that was derived from the CAD and MS^3 spectra of the ^{34}S-containing isotopomers. All spectra are reported in Tables 3 and 4. The $[COS-SO]^+$ and $[COS-S_2O]^+$ adducts show common spectral features, the most salient being the following: (i) the CAD spectra display $[M - CO]^+$ ions, namely S_2O^+ and S_3O^+, as the major fragments from the dissociation process

$$COS-SO^+\ (COS-S_2O^+) \rightarrow S_2O^+\ (S_3O^+) + CO \qquad (3)$$

(ii) $[M - CO_2]^+$ fragments from the metastable transition

$$COS-SO^+\ (COS-S_2O^+) \rightarrow S_2^+\ (S_3^+) + CO_2 \qquad (4)$$

display dish-topped peaks (Figure 2), whose kinetic energy releases amount to 866 ± 30 meV (S_2^+) and to 620 ± 10 meV (S_3^+). For comparison purposes $[COS-SO]^+$ and $[COS-S_2O]^+$ model ions were generated in the absence of O_3 by the SO_2/CI of COS, and their spectra, also reported in Tables 3 and 4, are indistinguishable from those of the species under study. Finally, S_nO^+ ($n = 1-5$) and S_n^+ ($n = 1-9$) ions were also detected in the O_3 chemical ionization of COS.

Confirming evidence was obtained by FT-ICR mass spectrometry, whereby the SO^+ ion, generated from neat SO_2 in the external ion source, isolated and then thermalized, was allowed to react with COS in the resonance cell, at pressures ranging from 4×10^{-8} to 1×10^{-7} Torr. The reactions

$$SO^+ + COS \xrightarrow{k_5} S_2O^+ + CO \xrightarrow{+COS} S_3O^+ + CO \qquad (5)$$
$$SO^+ + COS \xrightarrow{k_6} S_2^+ + CO_2 \qquad (6)$$

were observed, leading to S_3O^+ and S_2^+ as the major final

TABLE 1: Total Energies, Geometries, and Vibrational Frequencies (Intensities) of the $[COSO_3]^+$ Species: Total Energies in Hartree, Bond Lengths in Å, Angles in Deg, Frequencies in cm^{-1}, Intensities in km/mol

	1	2	3	TS(**2**→**3**)
E_{B3LYP}	−736.797663	−736.746697	−736.801153	−736.730078
ZPE[a]	0.014783	0.018281	0.016683	0.016926
$E_{CCSD(T)}$	735.589059	735.544609	735.599336	735.527715
	22.6 (0.7)	63.5 (3.8)	24.5 (0.7)	503.1*i*
	51.4 (0.2)	149.0 (5.9)	43.9 (1.7)	95.8
	77.2 (0.2)	327.8 (10.1)	58.8 (6.6)	177.7
	108.3 (10.1)	431.9 (45.2)	79.1 (4.7)	273.1
	118.2 (18.4)	511.8 (6.1)	179.2 (25.6)	324.7
	173.2 (27.9)	550.2 (9.4)	370.6 (8.3)	494.6
	205.7 (2.8)	590.6 (4.8)	503.0 (1.9)	543.1
	210.4 (3.6)	720.8 (15.0)	647.3 (30.9)	669.2
	373.4 (13.8)	841.3 (3.5)	660.3 (23.1)	768.5
	1251.2 (54.1)	885.8 (12.4)	1035.2 (71.1)	789.2
	1598.9 (186.5)	962.4 (48.1)	1347.7 (58.3)	1099.2
	2298.4 (37.1)	1989.7 (377.3)	2372.8 (955.6)	2194.7

	1	2		3		TS(**2**→**3**)
$r(C_2O_1)$	1.113	1.158	$r(C_2O_1)$	1.146	$r(C_2O_1)$	1.410
$r(S_3C_2)$	2.189	1.905	$r(O_3C_2)$	1.178	$r(O_3C_2)$	1.253
$\angle(S_3C_2O_1)$	178.1	126.6	$\angle(O_3C_2O_1)$	179.3	$\angle(O_3C_2O_1)$	154.0
$r(O_4S_3)$	1.445	1.592	$r(S_4O_3)$	2.583	$r(O_4O_3)$	1.563
$\angle(O_4S_3C_2)$	107.0	93.0	$\angle(S_4O_3C_2)$	137.2	$\angle(O_4O_3C_2)$	112.0
$\angle(O_4S_3C_2O_1)$	14.4	−177.1	$\angle(S_4O_3C_2O_1)$	180.0	$\angle(O_4O_3C_2O_1)$	156.4
$r(O_5O_4)$	3.083	1.490	$r(O_5S_4)$	1.650	$r(O_5O_4)$	1.408
$\angle(O_5O_4S_3)$	66.4	113.2	$\angle(O_5S_4O_3)$	91.7	$\angle(O_5O_4O_3)$	108.3
$\angle(O_5O_4S_3C_2)$	84.6	2.0	$\angle(O_5S_4O_3C_2)$	180.0	$\angle(O_5O_4O_3C_2)$	65.7
$r(O_6O_5)$	1.201	1.382	$r(O_6O_5)$	1.275	$r(S_6O_5)$	1.617
$\angle(O_6O_5O_4)$	74.2	110.6	$\angle(O_6O_5S_4)$	125.1	$\angle(S_6O_5O_4)$	113.5
$\angle(O_6O_5O_4S_3)$	173.3	−10.3	$\angle(O_6O_5S_4O_3)$	0.0	$\angle(S_6O_5O_4O_3)$	−57.1

[a] Zero point energy.

TABLE 2: Thermochemical Data (kcal mol^{-1}, 298 K) Relevant to the COS^+/O_3 System, Computed at the CCSD(T)/6-311+G (2d) Level of Theory

process	$\Delta H°$	barrier height
$COS^+ + O_3 \rightarrow$ **1**	−58.1	
1 → $CO + SO^+ + O_2(^3\Sigma_g^-)$	6.7	
$COS^+ + O_3 \rightarrow$ **2**	−29.9	
2 → **3**	−34.2	9.7
3 → $CO_2 + SOO^+$	5.9	
$SOO^+ \rightarrow SO^+ + O(^3P)$	−2.1	

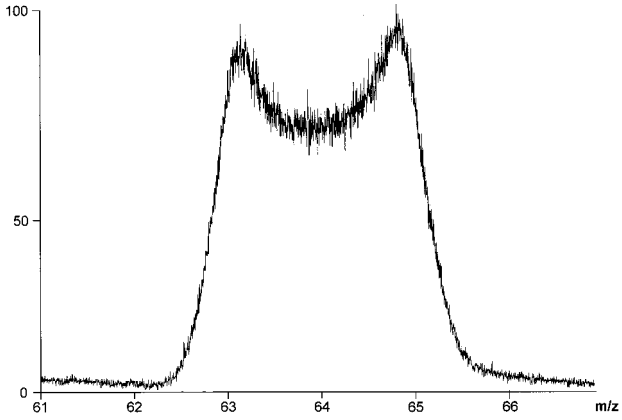

Figure 2. Dish-topped peak at *m*/*z* 64 from the metastable decomposition of the $[SO-COS]^+$ adduct.

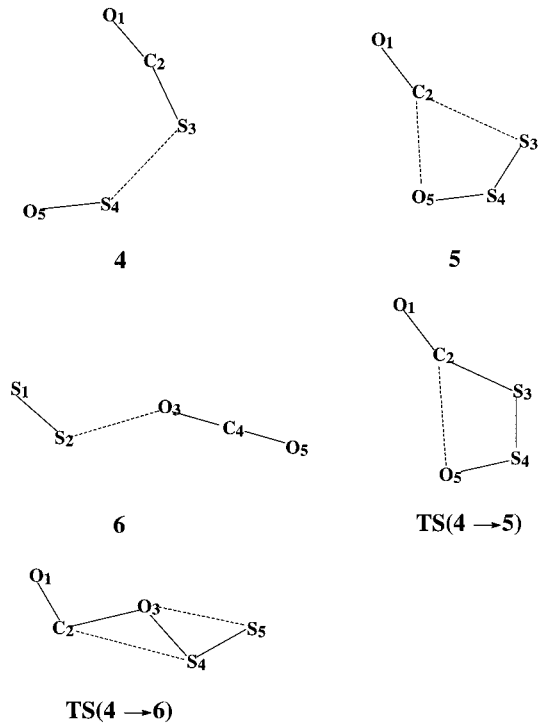

Figure 3. Optimized geometries of the localized minima on the potential energy surface of the SO^+/COS system. TS(**4** → **5**) and TS(**4** → **6**) are the transition states for the **4** → **5** and **4** → **6** isomerizations.

products. Furthermore, the S_2O^+ generated in the source by O_3/CI of COS, isolated and allowed to react with the COS in the cell undergoes the reaction

$$S_2O^+ + COS \xrightarrow{k_7} S_3O^+ + CO \qquad (7)$$

confirming the role of S_2O^+ as a precursor of S_3O^+ indirectly suggesting the transient formation of the $[COS{\cdot}SO]^+$ and $[COS{\cdot}S_2O]^+$ adducts, undetectable at the low pressures typical of the ICR experiments due, to their complete dissociation in the absence of efficient collisional stabilization. The measured rate coefficients amount to $k_5 \approx k_6 = (2.1 \pm 0.3) \times 10^{-10}$ cm^3 s^{-1} molecule $^{-1}$, the k_5/k_6 branching ratio being ca. 0.94 ± 0.1, and $k_{(7)} = (1.9 \pm 0.3) \times 10^{-10}$ cm^3 s^{-1} molecule $^{-1}$. From the k_{ADO} reaction rate constants, all the above values correspond to collisional efficiencies of ca. 10%.

TABLE 3: Collisionally Activated Dissociation (CAD) and MS³ Spectra of $[COS_2O]^+$ Ions from Different Sources

CAD										
COS/O_3				COS/SO_2						
m/z 108[b]		*m/z* 110[b]		*m/z* 108[b]		*m/z* 110[b]		MS³[a]		
m/z	*I* (%Σ)[c]	*m/z*	*I* (%Σ)	*m/z*	*I* (%Σ)	*m/z*	*I* (%Σ)	parent	daughter	fragment
80	22.7	82	22.9	80	23.2	82	21.8	*108*	80	64, 48, 32
64	8.1	66	7.5	64	7.0	66	7.5		64	32
		62	11.6			62	11.2		60	44, 32, 28, 12
60	23.4	60	11.6	60	24.2	60	11.2			
		50	18.4			50	19.4	*110*	82	66, 50,48, 34, 32
48	38.3	48	21.4	48	38.9	48	21.2		66	34, 32
46	<1	46	<1							
44	1.3	44	<1	44	1.0	44	<1			
		34	2.9			34	3.2			
32	5.3	32	2.9	32	4.9	32	3.4			
28	0.9	28	0.8	28	0.8	28	1.1			

[a] Significant spectra only are reported. [b] *m/z* of the $[COS_2O]^+$ and $[CO^{34}SSO]^+$ parent ions. [c] Percentage of the fragments intensity with respect to the total fragments intensities, standard deviation ± 10%.

TABLE 4: Collisionally Activated Dissociation (CAD) and MS³ Spectra of $[COS_3O]^+$ Ions from Different Sources

CAD										
COS/O_3				COS/SO_2						
m/z 140[b]		*m/z* 142[b]		*m/z* 140[b]		*m/z* 142[b]		MS³[a]		
m/z	*I* (%Σ)[c]	*m/z*	*I* (%Σ)	*m/z*	*I* (%Σ)	*m/z*	*I* (%Σ)	parent	daughter	fragment
112	34.2	114	32.8	112	34.2	114	32.9	*140*	96	64, 32
96	1.4	98	1.5	96	1.6	98	1.8		64	32
		82	22.6			82	22.6			
80	34.0	80	11.0	80	35.3	80	11.5	*142*	98	66, 34
		66	10.1			66	9.6		66	34, 32
64	15.3	64	6.0	64	14.4	64	6.3		64	32
		62	3.5			62	3.4			
60	9.0	60	5.8	60	8.7	60	5.6			
		50	1.8			50	1.7			
48	4.7	48	3.2	48	4.5	48	3.0			
		34	0.6			34	0.5			
32	1.4	32	1.1	32	1.3	32	1.0			

[a] Significant spectra only are reported. [b] *m/z* of the $[COS_3O]^+$ and $[CO^{34}SS_2O]^+$ parent ions. [c] Percentage of the fragments intensity with respect to the total fragments intensities, standard deviation ± 10%.

Passing to the theoretical results, Figure 3 reports the optimized geometries of the minima localized on the potential energy surface of the $[COS-SO]^+$ system. The total energies and frequencies are reported in Table 5, whereas the energetics of relevant processes, computed at the CCSD(T) level, are reported in Table 6. The ions **4**, **5**, and **6** can be essentially described as $[COS-SO^+]$, $[CO-S_2O^+]$, and $[CO_2-S_2^+]$ ion−molecule complexes. Ion **6** is the local minimum, ions **4** and **5** being less stable by 31.5 and 52.8 kcal mol^{-1}, respectively. The transition states for the **4** → **5** and **4** → **6** isomerization are also illustrated in Figure 3.

Discussion

The Formation of the SO^+ Ion. The experimental and theoretical evidence concur in identifying the reaction of COS^+ with O_3 as an effective route to the SO^+ ion. Although attempts at detecting the $[COS-O_3]^+$ intermediate failed, the mass spectrometric results undoubtedly support the formation of such an adduct as a transient species that is highly unstable toward dissociation. This evidence is supported by the computational results reported in Table 2 and is outlined in the energy profile of Figure 4. Both the precursor ions, **1**, whose formation appears entropically favored, and **2**, undergo dissociation processes whose energetic requirements are largely met by the energy released upon association of the reactants, and all eventually lead to SO^+ as the final product. The result is in line with previous evidence on the ozone reactivity toward gaseous ionic reagents,[4] that has characterized the O_3 molecule as an oxygen atom donor, as well as with the general tendency of the charged adducts formed to decompose, releasing good leaving groups. The presence of a preformed CO molecule in the COS^+ can lead to a prompt dissociation of the complex formed, which accounts for the failure to experimentally detect $[COS-O_3]^+$.

The SO^+ Reactivity toward COS. As reported in a previous paragraph, and consistent with a recent SIFT study,[17] the reaction of SO^+ with COS yields S_2O^+ and S_2^+ as the primary products according to the sequences

$$SO^+ + COS \longrightarrow [COS\text{-}SO]^+ \longrightarrow S_2O^+ + CO \quad (3)$$

$$[COS\text{-}SO]^+ \longrightarrow S_2^+ + CO_2 \quad (4)$$

This reaction pathway was firmly established by the detection and the structural assay of the $[COS-SO]^+$ complex that, in contrast with $[COS-O_3]^+$, is detectable under high-pressure CI conditions. However, the rich ion chemistry observed is only primed by SO^+, as the S_2O^+ ion formed further reacts with COS according to the general reaction sequences

$$S_nO^+ + COS \longrightarrow [COS_{n+1}O]^+ \longrightarrow S_{n+1}O^+ + CO \quad (8)$$

$$[COS_{n+1}O]^+ \longrightarrow S_{n+1}^+ + CO_2 \quad (9)$$

that can be viewed as chain oligomerization processes. Progres-

TABLE 5: Total Energies, Geometries, and Vibrational Frequencies (intensities) of the $[COS-SO]^+$ Species: Total Energies in Hartree, Bond Lengths in Å, Angles in Deg, Frequencies in cm^{-1}, Intensities in km/mol

	4	**5**	**6**	TS(**4**→**5**)	TS(**4**→**6**)
E_{B3LYP}	−984.690538	−984.645297	−984.735077	−984.639902	−984.621189
ZPE[a]	0.013193	0.011121	0.014029	0.010890	0.010980
$E_{CCSD(T)}$	−983.260846	−983.225914	−983.312166	−983.212749	−983.195943
	40.4 (4.4)	48.3 (0.5)	18.8 (0.7)	293.8*i*	142.7*i*
	103.7 (1.7)	73.1 (2.1)	50.7 (1.9)	31.2	81.3
	198.8 (6.2)	100.2 (3.1)	72.2 (14.1)	66.8	123.3
	295.1 (49.5)	102.5 (2.1)	154.7 (25.8)	124.7	125.9
	481.1 (4.3)	186.0 (21.8)	653.3 (31.3)	295.8	334.5
	500.3 (6.9)	344.9 (4.3)	665.9 (27.0)	352.8	446.8
	755.6 (35.8)	522.2 (44.4)	800.9 (10.4)	491.7	738.0
	1220.1 (86.5)	1224.4 (87.2)	1353.3 (59.7)	1188.5	815.7
	2195.9 (583.0)	2280.2 (56.6)	2388.5 (1080.0)	2228.6	2155.3

	4	**5**	TS(**4**→**5**)		**6**		TS(**4**→**6**)
$r(C_2O_1)$	1.132	1.117	1.119	$r(S_2S_1)$	1.842	$r(C_2O_1)$	1.126
$r(S_3C_2)$	1.626	2.687	2.185	$r(O_3S_2)$	2.592	$r(O_3C_2)$	1.760
$\angle(S_3C_2O_1)$	178.4	170.3	146.2	$\angle(O_3S_2S_1)$	106.7	$\angle(O_3C_2O_1)$	122.8
$r(S_4S_3)$	2.447	1.999	2.025	$r(C_4O_3)$	1.175	$r(S_4O_3)$	1.586
$\angle(S_4S_3C_2)$	95.0	95.6	102.1	$\angle(C_4O_3S_2)$	141.5	$\angle(S_4O_3C_2)$	115.4
$\angle(S_4S_3C_2O_1)$	−178.0	180.0	−115.8	$\angle(C_4O_3S_2S_1)$	180.0	$\angle(S_4O_3C_2O_1)$	180.0
$r(O_5S_4)$	1.454	1.447	1.454	$r(O_5C_4)$	1.147	$r(S_5S_4)$	1.865
$\angle(O_5S_4S_3)$	108.5	115.8	114.0	$\angle(O_5C_4O_3)$	179.4	$\angle(S_5S_4O_3)$	109.1
$\angle(O_5S_4S_3C_2)$	89.3	0.0	34.0	$\angle(O_5C_4O_3S_2)$	180.0	$\angle(S_5S_4O_3C_2)$	180.0

[a] Zero point energy.

TABLE 6. Thermochemical Data (kcal mol^{-1}, 298 K) Relevant to the SO^+/COS System, Computed at the CCSD(T)/6-311+G (2d) Level of Theory

process	$\Delta H°$	barrier height
$SO^+ + COS \rightarrow$ **4**	−26.5	
4 → **5**	21.3	28.9
4 → **6**	−31.5	39.2
5 → $CO + S_2O^+$	6.8	
6 → $CO_2 + S_2^+$	5.7	

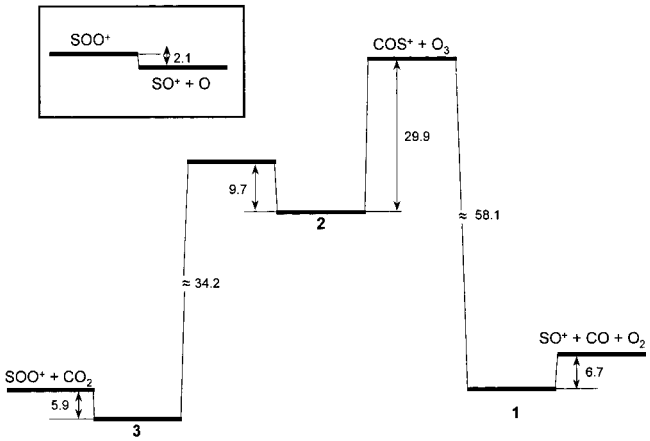

Figure 4. Energy profile relevant to the potential energy surface of the COS^+/O_3 system.

sion of reaction 8 beyond $n = 1$ is demonstrated by the actual observation of the $[COS-S_2O]^+$ complex and of its dissociation product, S_3O^+, as well as by the observation of reaction 7 in FT-ICR experiments. Further progress of reaction 8 is demonstrated by the observation of the S_4O^+ and S_5O^+ ions, although detection of their $[COS_{n+1}O]^+$ precursors proved difficult, even under high-pressure conditions, since they become increasingly unstable toward dissociation by processes such as (8) and (9); as the *n* value is increased their steady-state abundance is reduced.

Unlike sequence (8), sequence (9) does not represent the exclusive route to the S_n^+ ions present in the source, the alternative pathway being the consecutive addition of S_{n+1}^+ ions

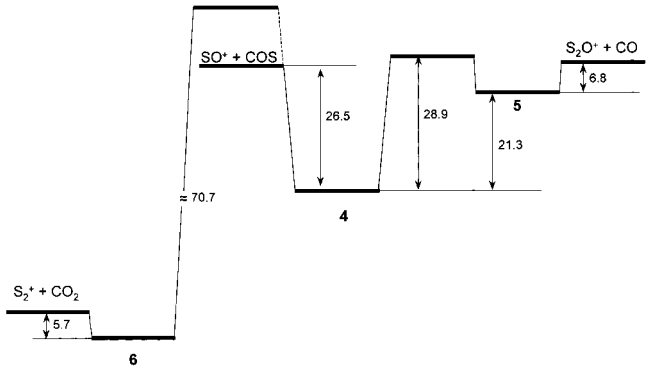

Figure 5. Energy profile relevant to the potential energy surface of the SO^+/COS system.

to COS.[18] The progression of reaction 9 over $n = 1$ cannot be directly demonstrated; nevertheless, both the complexes observed, $[COSSO]^+$ and $[COSS_2O]^+$, undergo this process by metastable transitions that are characterized by a large barrier for the reverse reaction, which points to an extensive molecular reorganization. Interestingly, under ICR conditions SO^+ undergoes both reactions 8 and 9 with COS, whereas S_2O^+ undergoes only reaction 8.

As for the process promoted by SO^+, the experimental branching ratio indicates that reactions 8 and 9 occur at a comparable rate, in agreement with previous results.[17] The theoretical results support the experimental evidence, as illustrated by the energy profile of Figure 5, which shows that reactions 8 and 9 involve ions that are formed upon isomerization of ion **4**, like **5** and **6**, that are structurally liable to decomposition into S_2O^+ and S_2^+, respectively. In particular, the **4** → **6** isomerization is characterized by a barrier to the reverse reaction as high as 70.7 kcal mol^{-1}, due both to the large endothermicity and to a purely kinetic component that reflects the extensive molecular reorganization required. The theoretically computed barrier is consistent with the fraction of energy released as translational energy of the fragments, experimentally found to amount to ca. 20 kcal mol^{-1}. In addition, the difference, 10.3 kcal mol^{-1}, between the theoreti-

cally computed heights of the barriers to the **4** → **5** and **4** → **6** isomerizations is not unduly large so as to be inconsistent with the experimentally observed occurrence of *both* reactions 8 and 9 under ICR conditions.

A different situation prevails in the S_2O^+/COS system, where process (9) is not observed at all under FT-ICR conditions. This can reasonably be traced to the more favorable geometry of the TS expected for the **4** → **5** isomerization, and hence to the lower height of the barrier to formation of the $[CO-S_3O]^+$ complex, whose dissociation eventually leads to S_3O^+. On the other hand, the smaller kinetic energy release measured for the metastable formation of S_3^+ rather than S_2^+ may be traced to the lower interaction energy of the monomers in $[CO_2-S_3]^+$, due to the lower charge density of S_3^+ than S_2^+.

Conclusions

Ionization of gaseous COS/O_3 mixtures has been identified as a source of SO^+ ions. The study of the SO^+ reactivity toward COS under chemical ionization conditions has revealed the operation of chain oligomerization reactions, leading to $S_{n+1}O^+$ and S_{n+1}^+ ions ($n = 1-4$). The theoretical evidence supports the experimental results and provides a picture that is consistent with the experimental trends observed.

Acknowledgment. Financial support from Ministero dell' Università e della Ricerca Scientifica e Tecnologica (MURST), from Consiglio Nazionale delle Ricerche (CNR), and from the Rome University "La Sapienza" is gratefully acknowledged. The authors thank F. Angelelli and A. Di Marzio for their helpful assistance.

References and Notes

(1) Kellog, W. W.; Cadle, R. D.; Allen, E. R.; Lazrus, A. L.; Martell, E. A. *Science* **1972**, *175*, 587. Sze, N. D.; Ko, M. K. W. *Atmos. Environ.* **1990**, *14*, 1223. Andreae, M. O.; Crutzen, P. J. *Science* **1997**, *276*, 1052.

(2) Smith, D.; Spanel, D. *Mass Spectrom. Rev.* **1995**, *14*, 255.

(3) Cacace, F.; Speranza, M. *Science* **1994**, *265*, 208. Mendes, M. A.; Moraes, L. A. B.; Sparrapan, R.; Eberlin, M. N.; Kostiainen, R.; Kotiaho T. *J. Am. Chem. Soc.* **1998**, *120*, 7869. Cacace, F.; Cipollini, R.; de Petris, G.; Pepi, F.; Rosi, M.; Sgamellotti, A. *Inorg. Chem.* **1998**, *37*, 1398.

(4) Cacace, F.; de Petris, G.; Pepi, F.; Rosi, M.; Sgamellotti, A. *Angew. Chem., Int. Ed.* **1999**, *38*, 2408. Cacace, F.; de Petris, G.; Pepi, F.; Rosi, M.; Troiani, A. *Chem.-Eur. J.* **2000**, *6*, 2572.

(5) Caravatti, P.; Allemann, M. *Org. Mass Spectrom.* **1991**, *26*, 514.

(6) Bartmess, J. E.; Georgiadis, R. M. *Vacuum* **1983**, *33*, 149.

(7) Becke, A. D. *J. Phys. Chem.* **1993**, *98*, 5648.

(8) Stevens, P. J.; Devlin, F. J.; Chablowski, C. F.; Frisch, M. J. *J. Phys. Chem* **1994**, 98, 11623.

(9) Mannfors, B.; Koskinen, J. T.; Pietila, L.-O.; Ahjopalo, L. *J. Mol. Struct. (Theoch)* **1997**, *39*, 393.

(10) Bauschlicher, C. W.; Ricca, A.; Partridge, H.; Langhoff, S. R. In *Recent Advances in Density Functional Theory*; Chong, D. P., Ed.; World Scientific Publishing Co.: Singapore, 1997; Part II.

(11) Bartlett, R. J. *Annu. Rev. Phys. Chem.* **1981**, *32*, 359.

(12) Olsen, J.; Jorgensen, P.; Koch, H.; Balkova, A.; Bartlett, R. J. *J. Chem. Phys.* **1996**, *104*, 8007.

(13) Raghavachari, K.; Trucks, G. W.; Pople, J. A.; Head-Gordon, M. *Chem. Phys. Lett.* **1989**, *157*, 479.

(14) Peng, C.; Schlegel, H. B. *Isr. J. Chem.* **1993**, *33*, 449. Peng, C.; Ayala, P. Y.; Schlegel, H. B.; Frisch, M. J. *J. Comput. Chem.* **1996**, *17*, 49.

(15) Krishnam, R.; Binkley, J. S.; Seeger, R.; Pople, J. A. *J. Chem. Phys.* **1980**, *72*, 650. McLean, A. D.; Chandler, G. S. *J. Chem. Phys.* **1980**, *72*, 5639. Clark, T.; Chandrasekhar, J.; Spitznagel, G. W.; Schleyer, P. v. R. *J. Comput. Chem.* **1983**, *4*, 294. Frisch, M. J.; Pople, J. A.; Binkley, J. S. *J. Chem. Phys.* **1984**, *80*, 3265.

(16) Frisch, M. J.; Trucks, G. W.; Schlegel, H. B.; Scuseria, G. E.; Robb, M. A.; Cheeseman, J. R.; Zakrewski, V. G.; Montgomery, J. A., Jr.; Stratmann, R. E.; Burant, J. C.; Dapprich, S.; Millam, J. M.; Daniels, A. D.; Kudin, K. N.; Strain, M. C.; Farkas, O.; Tomasi, J.; Barone, V.; Cossi, M.; Cammi, R.; Mennucci, B.; Pomelli, C.; Adamo, C.; Clifford, S.; Ochterski, J.; Petersson, G. A.; Ayala, P. Y.; Cui, Q.; Morokuma, K.; Malick, D. K.; Rabuck, A. D.; Raghavachari, K.; Foresman, J. B.; Cioslowski, J.; Ortiz, J. V.; Baboul, A. G.; Stefanov, B. B.; Liu, G.; Liashenko, A.; Piskorz, P.; Komaromi, I.; Gomperts, R.; Martin, R. L.; Fox, D. J.; Keith, T.; Al-Laham, M. A.; Peng, C. Y.; Nanayakkara, A.; Gonzalez, C.; Challacombe, M.; Gill, P. M. W.; Johnson, B.; Chen, W.; Wong, M. W.; Andres, J. L.; Head-Gordon, M.; Repogle, E. S.; Pople, J. A. *Gaussian 98*, Revision A.7; Gaussian, Inc.: Pittsburgh, PA, 1998.

(17) Decker, B. K.; Adams, N. G.; Babcock L. M. *Int. J. Mass Spectrom.* **2000**, *195*, 185.

(18) Smith, D.; Adams, N. G.; Lindinger W. *J. Chem. Phys.* **1981**, *75*, 3365. Decker, B. K.; Babcock, L. M.; Adams, N. G. *J. Chem. Phys.* **2000**, *104*, 801.